Zhang *et al.*
EURASIP Journal on Advances in Signal Processing (2023) 2023:39
https://doi.org/10.1186/s13634-023-00997-1

EURASIP Journal on Advances in Signal Processing

RESEARCH Open Access

Joint range, angle and polarization estimation in polarimetric FDA-MIMO radar based on Tucker tensor decomposition

Qi Zhang, Hong Jiang* and Yunchang Liu

*Correspondence:
jiangh@jlu.edu.cn

College of Communication Engineering, Jilin University, 130012 Changchun, China

Abstract

Frequency diverse array multiple-input multiple-output (FDA-MIMO) radar is an emerging technology to offer range-angle-dependent beampattern. Polarimetric FDA-MIMO radar can sense additional polarization information to improve target identification capability. In this article, we investigate the problem of joint range, angle and polarization parameter estimation in a monostatic polarimetric FDA-MIMO radar with an FDA at transmitter and a cross-dipole array at receiver. Unlike the conventional methods in which the multidimensional data structure is rearranged into vectors or matrices by stacking operation, we propose a Tucker tensor decomposition-based scheme, which can reserve the original data structure and avoid spoiling the inherent characteristics of interest, especially when the number of snapshots is small. The third-order tensor model of the observed data is constructed. Two approaches named as Tucker covariance reconstruction and Tucker signal subspace are presented using the fourth-order covariance tensor decomposition. The Cramér–Rao bound for range, angle and polarization estimation is also provided. Numerical experiments demonstrate the superiorities of the proposed approaches. Specifically, two targets with identical range and close angles are effectively distinguished.

Keywords: FDA-MIMO radar, Tucker tensor decomposition, Range-angle-polarization estimation, Polarization sensitive array, Signal subspace

1 Introduction

Multiple-input multiple-output (MIMO) radar [1] is a powerful technique for target detection, localization and imaging. MIMO radar array with colocated sensors has strong capability of estimating the angles of targets [2, 3]. However, with conventional MIMO radar, two targets having different angles but same range cannot be directly identified. Frequency diverse array (FDA), as an emerging scheme which was first proposed in [4], has received much attention in recent years. The carrier frequency of FDA has a small frequency increment between contiguous elements. Base on this design, it can produce angle-range-dependent transmit beampattern [5, 6]. In [7], the FDA radar data processing method has been introduced systematically. FDA is widely suggested for joint angle-range localization of targets. In [8], the FDA sensors are divided into multiple

subarrays and the transmit beamspace matrix is optimized with the use of convex optimization. In [9], a subarray scheme on FDA radar has been devised for range and angle estimation. A simple range-angle localization of targets by uniform linear array (ULA) double-pulse FDA radar has been proposed in [10]. FDA-MIMO radar [11–13], as a combination of FDA technology and MIMO radar, has received much attention and been investigated in many topics such as target detection [14, 15], jammer suppression [16], parameter estimation [17] and resolution evaluation [18], etc. Typically, the researches on joint parameter estimation in FDA-MIMO radar focus on some efficient solutions given by subspace-based methods, such as MUSIC, ESPRIT and combined MUSIC-ESPRIT [19–21]. In [22], the ambiguity function and ESPRIT based method has been presented for FDA-MIMO radar target localization. In [23], a real-valued subspace decomposition method has been proposed for joint angle and range estimation in bistatic FDA-MIMO radar. A joint range, angle and Doppler estimation method for FDA-MIMO radar has been introduced [24], in which 3D search problem is simplified into three 1D search problems which reduces the computation complexity. In [25], a spatial smoothing technique combined with ESPRIT algorithm has been proposed to obtain angle, range and velocity in FDA-MIMO radar. Different from these methods, atomic norm-based method has also been proposed to solve the range-angle estimation problem [26–28].

In practice, due to the reflected signals composed of electric and magnetic components, polarization diversity is of great significance in target identification when multiple targets are so closely spaced that they cannot be distinguished well in spatial domain. The multi-parameter estimation problem in the polarimetric MIMO radar have been investigated, e.g., in [29–33]. More recently, the FDA-MIMO radar with polarization sensitive array, which consider polarization information combined with range and angle information, has been studied in [34–36], which can improve the performance of target identification and increase the angle-range-polarization resolution. A sparse reconstruction beamforming method has been presented in [34]. A successive ESPRIT algorithm has been developed to estimate the angle-range-polarization parameters in [35]. In [36], a sparse polarization sensitive FDA-MIMO radar with co-prime frequency offsets has been explored based on successive propagator method.

Despite the fact that the performance of FDA-MIMO radar multiple parameter estimation has been improved in the aforementioned approaches, the multidimensional structure is rearranged into matrices by means of stacking operation. Thus, the original data structure cannot be reserved well, resulting in the damage of the inherent characteristics of interest, especially when the number of snapshots is small. Recently, the tensor-based algorithm has received much attention as a more natural approach to store and manipulate multidimensional data. In [37], a broad overview of tensor analysis has been provided in wireless communications and MIMO radar including basic tensor operations, common tensor decompositions. The higher-order extensions of the singular value decomposition (SVD), i.e., HOSVD [38], as a Tucker tensor model [39], has played an important role in tensor signal processing. Several Tucker tensor-based methods have been proposed such as in [40–44] to obtain the direction-of-departure and direction-of-arrival estimation in bistatic MIMO radar using the HOSVD and covariance matrix

reconstruction. The use of tensor representation allows us to further exploit the structure inherent in the array data.

In this article, we investigate the problem of joint range, angle and polarization parameter estimation based on Tucker tensor decomposition in a monostatic polarimetric FDA-MIMO radar system. First, we develop a third-order tensor signal model for polarimetric FDA-MIMO radar. Then, we, respectively, present two approaches named as Tucker covariance reconstruction (TCR) and Tucker signal subspace (TSS) to jointly estimate the range, angle and polarization parameters of targets. We construct the fourth-order covariance tensor, perform its truncated HOSVD for eigenstructure extraction, and utilize multiple shift-invariance operations to achieve the range-angle-polarization parameters with proper pairing. The detailed analyses concerning complexity as well as Cramér–Rao bound (CRB) for range, angle and polarization estimation are also provided. The performance of the two proposed algorithms are compared with that of the existing ESPRIT method in numerical experiments. The proposed tensor-based algorithms utilize the inherent multidimensional properties and avoid the matrix stacking operation that may bring error accumulation. Thus, the estimation accuracies can be enhanced especially when the number of snapshots is small. Furthermore, polarization diversity is exploited in FDA-MIMO radar to distinguish multiple targets with close angles or close ranges, which can improve the capability of multi-target identification in FDA-MIMO radar.

The rest of this article is organized as follows. The preliminaries of tensor are introduced in Sect. 2. The methods are described in Sect. 3, in which a tensor signal model for polarimetric FDA-MIMO radar is developed, the Tucker tensor decomposition-based algorithms for joint angle, range and polarization estimation are presented, and the performance analysis is given including the algorithm complexity and CRB. In Sect. 4, the simulation results and discussion are given to verify the effectiveness of the proposed tensor-based algorithms. Finally, a conclusion is drawn in Sect. 5.

Notations: To facilitate the distinction between scalars, matrices, and tensors, the following notation is used: Scalars are denoted as italic letters, column vectors as lowercase bold-face letters, matrices as bold-face capitals, and tensors are written as bold-face calligraphic letters. The superscript$(\cdot)^T$, $(\cdot)^H$ and $(\cdot)^*$ denote transpose, Hermitian transpose and conjugate operators, respectively; diag$(\cdot)$ denotes the diagonalization operation, rank $(\cdot)$ and det$(\cdot)$ denote rank operator and the determinant of a matrix, respectively. vec$(\cdot)$ denotes the vectorization operator, tr$(\cdot)$ is the trace operator. ang$(\cdot)$ denotes the angle operator and Re$(\cdot)$ is the real part operator of a complex number.

2 Preliminaries

A tensor is a multidimensional array [45]. An N-th order tensor can be expressed as $\boldsymbol{\mathcal{X}} \in \mathbb{C}^{I_1 \times I_2 \times \cdots \times I_N}$. The fibers are the higher-order analog of matrix rows and columns. The tensor operations in our paper are consistent with [46] which are listed as follows:

Unfolding or Matricization of the tensors. The mode-n unfolding of an N-th order tensor $\boldsymbol{\mathcal{X}} \in \mathbb{C}^{I_1 \times I_2 \times \cdots \times I_N}$ is denoted by $[\boldsymbol{\mathcal{X}}]_{(n)}$. The $(i_1, i_2, \cdots, i_N)$-th element of $\boldsymbol{\mathcal{X}}$ maps to the (i_n, j)-th element of $[\boldsymbol{\mathcal{X}}]_{(n)}$, where $j = 1 + \sum_{k=1, k\neq n}^{N} (i_k - 1) J_k$ with $J_k = \prod_{m=1, m\neq n}^{k-1} I_m$.

Moreover, a matrix unfolding of the tensor $\boldsymbol{\mathcal{X}}$ along the n-th mode is denoted by $[\boldsymbol{\mathcal{X}}]_{(n)}$ and can be understood as a matrix containing all the n-mode vectors of the tensor $\boldsymbol{\mathcal{X}}$. The order of the columns is chosen in accordance with [46].

The n-mode inner product of a tensor $\boldsymbol{\mathcal{X}} \in \mathbb{C}^{I_1 \times I_2 \times \cdots \times I_N}$ and a tensor $\boldsymbol{\mathcal{Y}} \in \mathbb{C}^{J_1 \times J_2 \times \cdots \times J_M}$ is defined, when $I_n = J_n$, $n \leq \min\{M, N\}$, it is given by $\boldsymbol{\mathcal{Z}} = \boldsymbol{\mathcal{X}} \bullet_n \boldsymbol{\mathcal{Y}} \in \mathbb{C}^{I_1 \times I_2 \times \cdots \times I_{n-1} \times I_{n+1} \times \cdots \times I_N \times J_1 \times J_2 \times \cdots \times J_{n-1} \times J_{n+1} \times \cdots \times J_M}$, where

$$z_{i_1,i_2,\ldots,i_{n-1},i_{n+1},\ldots,i_N,j_1,j_2,\ldots,j_{n-1},j_{n+1},\ldots,j_M} = \sum_{i_n=1}^{I_n} x_{i_1,i_2,\ldots,i_N} \cdot y_{j_1,j_2,\ldots,j_{n-1},i_n,j_{n+1},\ldots,j_M} \tag{1}$$

The n-mode product of a tensor $\boldsymbol{\mathcal{X}} \in \mathbb{C}^{I_1 \times I_2 \times \cdots \times I_N}$ and a matrix $\mathbf{A} \in \mathbb{C}^{J_n \times I_n}$ along the n-th mode is denoted as $\boldsymbol{\mathcal{Y}} = \boldsymbol{\mathcal{X}} \times_n \mathbf{A} \in \mathbb{C}^{I_1 \times I_2 \times \cdots \times I_{n-1} \times J_n \times I_{n+1} \times \cdots \times I_N}$, which is calculated by

$$y_{i_1,i_2,\cdots,i_{n-1},j_n,i_{n+1},\cdots,i_N} = \sum_{i_n=1}^{I_n} x_{i_1,i_2,\cdots,i_N} \cdot a_{j_n,i_n} \tag{2}$$

It may be visualized by multiplying all n-mode vectors of $\boldsymbol{\mathcal{X}}$ from the left-hand side by the matrix $\mathbf{A}$. The mode-n product admits the following properties:

$$\boldsymbol{\mathcal{Y}} = \boldsymbol{\mathcal{X}} \times_n \mathbf{A} \Leftrightarrow [\boldsymbol{\mathcal{Y}}]_{(n)} = \mathbf{A}[\boldsymbol{\mathcal{X}}]_{(n)} \tag{3}$$

$$\begin{cases} \boldsymbol{\mathcal{X}} \times_n \mathbf{A} \times_m \mathbf{B} = \boldsymbol{\mathcal{X}} \times_m \mathbf{B} \times_n \mathbf{A}, \ m \neq n \\ \boldsymbol{\mathcal{X}} \times_n \mathbf{A} \times_n \mathbf{B} = \boldsymbol{\mathcal{X}} \times_n (\mathbf{BA}) \end{cases} \tag{4}$$

$$[\boldsymbol{\mathcal{Y}}]_{(n)} = \mathbf{A}_n \cdot [\boldsymbol{\mathcal{X}}]_{(n)} \cdot [\mathbf{A}_{n+1} \otimes \cdots \otimes \mathbf{A}_N \otimes \mathbf{A}_1 \cdots \otimes \mathbf{A}_{n-1}] \tag{5}$$

The higher-order SVD (HOSVD) or Tucker decomposition of a tensor $\boldsymbol{\mathcal{X}} \in \mathbb{C}^{I_1 \times I_2 \times \cdots \times I_N}$ is given by

$$\boldsymbol{\mathcal{X}} = \boldsymbol{\varsigma} \times_1 \mathbf{A}_1 \times_2 \mathbf{A}_2 \times \ldots \mathbf{A}_N \tag{6}$$

where $\boldsymbol{\varsigma} \in \mathbb{C}^{J_1 \times J_2 \times \cdots \times J_N}$ is the core tensor which satisfies the all-orthogonality conditions [46] and $\mathbf{A}_n \in \mathbb{C}^{I_n \times J_n}, n = 1, 2, \cdots N$, are the unitary matrices of n-mode singular vectors.

3 Methods

3.1 Tensor signal model of polarimetric FDA-MIMO radar

As illustrated in Fig. 1, we consider a monostatic polarimetric FDA-MIMO radar equipped with a transmit FDA having M sensors and a receive array having N cross-dipole sensors, both are uniform linear arrays. Assume that the antennas are of ideal, identical isotropic sensors, and the range of targets is much larger than the apertures of transmit and receive arrays. The transmit array with M sensors simultaneously send M waveforms with identical bandwidth but different frequencies. Taking the first transmit sensor as the reference sensor, the carrier frequency of the m-th sensor is

$$f_m = f_0 + (m-1)\Delta f, \ m = 1, \cdots, M \tag{7}$$

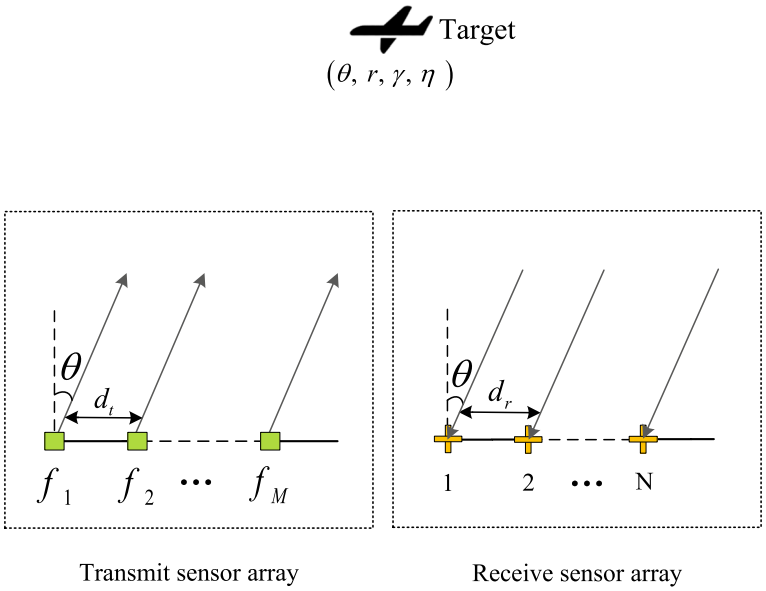

Fig. 1 A monostatic polarimetric FDA-MIMO radar with a transmit FDA having *M* sensors and a receive array having *N* cross dipole sensors

where f_0 is the reference frequency, and Δf denotes the frequency increment between adjacent array sensors which is far less than the frequency f_0. The transmitting signal of the m-th sensor can be expressed as

$$s_m(t) = \psi_m(t)e^{j2\pi f_m t}, 0 \le t \le T \tag{8}$$

where $\psi_m(t)$ is the baseband waveform envelope, and T is the radar pulse duration. It is assumed that the transmitted M waveforms of each sensor are orthogonal to each other.

For the p-th far-field target, $p = 1, 2, \cdots, P$, assume that it is localized at angle θ_p and range r_p. The propagation time from the m-th transmit sensor to the n-th receive sensor can be written as

$$\tau(m, n, \theta_p, r_p) = \frac{2r_p}{c} - \frac{d_t(m-1)\sin\theta_p}{c} - \frac{d_r(n-1)\sin\theta_p}{c} \tag{9}$$

where d_t and d_r, respectively, denote the inter-sensor spacing at the transmitter and receiver, which are no more than half a wavelength $\lambda_0 = c/f_0$, with c being the propagation speed. $2r_p/c$ is the common propagation time delay, and the next two terms represent the time shifts brought by the transmitter and receiver arrays, respectively.

At the receiver array of the polarimetric FDA-MIMO radar, the cross-dipoles are used to measure the polarization states of a transverse electromagnetic (TEM) wave and improve target identification capability by exploiting polarization diversity. The polarization state of TEM wave can be represented by parameters (γ, η), which are two phase descriptors of a polarized signal [47, 48]. Thus the complex electric field vector is

$$\mathbf{e} = A\begin{bmatrix} \cos\gamma \\ \sin\gamma e^{j\eta} \end{bmatrix} \tag{10}$$

where A is the electric field amplitude. $\tan\gamma$ represents the ratio of the electric field amplitude in the X direction to that in the Y direction, $\gamma \in \left[0, \frac{\pi}{2}\right]$, and η signifies the phase difference between the electric fields in the Y direction and X direction, $\eta \in [-\pi, \pi]$.

Under the assumption of narrow-band and far-field signals, the signals are reflected by P far-field targets. With a cross-dipole uniform linear array used at the receiver, the polarization vector for the p-th target can be written as

$$\begin{aligned}\mathbf{v}(\theta_p, \gamma_p, \eta_p) &= \begin{bmatrix} -1 & 0 \\ 0 & \cos\theta_p \end{bmatrix} \begin{bmatrix} \cos\gamma_p \\ \sin\gamma_p e^{j\eta_p} \end{bmatrix} \\ &= \begin{bmatrix} -\cos\gamma_p \\ \sin\gamma_p \cos\theta_p e^{j\eta_p} \end{bmatrix}\end{aligned} \tag{11}$$

where $0 \le \gamma_p \le \pi/2$, $-\pi \le \eta_p < \pi$. Thus, the received signal from the m-th transmit sensor to the n-th cross-dipole sensor can be expressed as

$$\mathbf{r}_{mn}(t) = \sum_{p=1}^{P} \psi_m(t - \tau(m, n, \theta_p, r_p)) e^{j2\pi f_m(t-\tau(m,n,\theta_p,r_p))} \mathbf{v}(\theta_p, \gamma_p, \eta_p) \tag{12}$$

In noisy environment, after sampling, recombination and matched filtering with the orthogonal transmit waveform $\psi_m(t)$, the output of a polarimetric FDA-MIMO radar can be reformulated as

$$\begin{aligned}\mathbf{y}_{m,n,l} = &\sum_{p=1}^{P} {\beta_p}^{(l)} e^{j2\pi(m-1)((d_t/\lambda_0)\sin\theta_p - (\Delta f/c)2r_p)} \\ &\times e^{j2\pi(n-1)(d_r/\lambda_0)\sin\theta_p} \mathbf{v}(\theta_p, \gamma_p, \eta_p) + \mathbf{z}_{m,n,l}\end{aligned} \tag{13}$$

for $m = 1, 2, \cdots, M$; $n = 1, 2, \cdots, N$, and $l = 1, 2, \cdots, L$, where L is the number of snapshots. $\beta_p^{(l)}$ is the complex scattering coefficient of the p-th target in the l-th snapshot. $\mathbf{y}_{m,n,l}$ and $\mathbf{z}_{m,n,l}$ denote the output data and noise with respect to the m-th transmit sensor, n-th receive sensor and the l-th snapshot, respectively.

In a conventional way, $\mathbf{y}_{m,n,l}$ is first arranged into a matrix $\mathbf{Y}^{(l)} \in \mathbb{C}^{2N\times M}$ as

$$\begin{aligned}\mathbf{Y}^{(l)} &= \sum_{p=1}^{P} {\beta_p}^{(l)} \mathbf{a}_r(\theta_p) \otimes \mathbf{v}(\theta_p, \gamma_p, \eta_p) \mathbf{a}_t^T(\theta_p, r_p) + \mathbf{Z}^{(l)} \\ &= \mathbf{A}_r(\theta) \otimes \mathbf{V}(\theta, \gamma, \eta) \mathrm{diag}(\mathbf{b}^{(\mathrm{l})}) \mathbf{A}_{\mathrm{t}}^{\mathrm{T}}(\theta, \mathrm{r}) + \mathbf{Z}^{(\mathrm{l})}\end{aligned} \tag{14}$$

where $\mathbf{b}^{(l)} = [\beta_1^{(l)}, \cdots, \beta_P^{(l)}]$ denotes the complex scattering coefficient vector related to the radar cross section (RCS). $\mathbf{Z}^{(l)}$ represents a Gaussian white noise matrix. $\mathbf{V}(\theta, \gamma, \eta) = [\mathbf{v}(\theta_1, \gamma_1, \eta_1), \cdots, \mathbf{v}(\theta_P, \gamma_P, \eta_P)] \in \mathbb{C}^{2\times P}$. $\mathbf{A}_t(\theta, r) = [\mathbf{a}_t(\theta_1, r_1), \mathbf{a}_t(\theta_2, r_2), \cdots, \mathbf{a}_t(\theta_P, r_P)] \in \mathbb{C}^{M\times P}$. $\mathbf{A}_r(\theta) = [\mathbf{a}_r(\theta_1), \mathbf{a}_r(\theta_2), \cdots, \mathbf{a}_r(\theta_P)] \in \mathbb{C}^{N\times P}$. The p-th steering vector $\mathbf{a}_t(\theta_p, r_p)$ of the transmit array can be written as

$$\mathbf{a}_t(\theta_p, r_p) = [1, e^{j2\pi((d_t/\lambda_0)\sin\theta_p - (\Delta f/c)2r_p)}, \cdots, e^{j2\pi(M-1)((d_t/\lambda_0)\sin\theta_p - (\Delta f/c)2r_p)}]^T \tag{15}$$

and the p-th steering vector $\mathbf{a}_r(\theta_p)$ of the receive array can be written as

$$\mathbf{a}_r(\theta_p) = \left[1, e^{j2\pi(d_r/\lambda_0)\sin\theta_p}, \cdots, e^{j2\pi(N-1)(d_r/\lambda_0)\sin\theta_p}\right]^T \tag{16}$$

By the vectorization of $\mathbf{Y}^{(l)}$, the observed matrix can be rewritten as a $2MN \times L$ vector $\mathbf{y}^{(l)} = \mathbf{A}(\theta, \phi, \gamma, \eta)\mathbf{b}^{(l)} + \mathbf{z}^{(l)}$, where $\mathbf{z}^{(l)}$ denotes the noise vector, whose elements are white Gaussian distributed with mean zero and variance σ. $\mathbf{A}(\theta, r, \gamma, \eta) = [\mathbf{a}_1(\theta, r, \gamma, \eta), \cdots, \mathbf{a}_P(\theta, r, \gamma, \eta)] \in \mathbb{C}^{2MN\times P}$ represents the joint transmit-receive-polarization steering matrix, with

$$\mathbf{a}_p(\theta, r, \gamma, \eta) = \mathbf{a}_t(\theta_p, r_p) \otimes \mathbf{a}_r(\theta_p) \otimes \mathbf{v}(\theta_p, \gamma_p, \eta_p) \tag{17}$$

where $\otimes$ denotes the Kronecker product. Then, the data in L snapshots for $\mathbf{y}^{(l)}$ are collected to form a matrix $\mathbf{Y} \in \mathbb{C}^{2MN\times L}$,

$$\mathbf{Y} = \mathbf{A}(\theta, r, \gamma, \eta)\mathbf{B} + \mathbf{Z} \tag{18}$$

where $\mathbf{Y} = \left[\mathbf{y}^{(1)}, \cdots, \mathbf{y}^{(L)}\right]$, $\mathbf{B} = \left[\mathbf{b}^{(1)}, \cdots, \mathbf{b}^{(L)}\right]$ and $\mathbf{Z} = \left[\mathbf{Z}^{(1)}, \cdots, \mathbf{Z}^{(L)}\right]$ represent the observation matrix, target scattering matrix and noise matrix, respectively, and

$$\begin{aligned}\mathbf{A}(\theta, r, \gamma, \eta) &= \mathbf{A}_t(\theta, r) \diamond \mathbf{A}_r(\theta) \diamond \mathbf{V}(\theta, \gamma, \eta) \\ &= \mathbf{A}_t(\theta, r) \diamond \tilde{\mathbf{A}}_r(\theta, \gamma, \eta)\end{aligned} \tag{19}$$

where $\diamond$ represents the Khatri–Rao product.

Note that the signal model in (18) is expressed as the form of a matrix via a stacking operation. Such a highly structured matrix cannot completely capture the inherent multidimensional structure. In our paper, $\mathbf{y}_{m,n,l}$ in (13) is directly arranged into a third-order tensor $\boldsymbol{\mathcal{Y}} \in \mathbb{C}^{M\times 2N\times L}$, then

$$\boldsymbol{\mathcal{Y}} = \boldsymbol{\iota} \times_1 \mathbf{A}_t \times_2 \tilde{\mathbf{A}}_r \times_3 \mathbf{B} + \boldsymbol{\mathcal{Z}} \tag{20}$$

where $\boldsymbol{\iota} \in \mathbb{C}^{P\times P\times P}$ is an identity tensor. Obviously, we have $\mathbf{Y} = [\boldsymbol{\mathcal{Y}}]^T_{(3)}$ and $\mathbf{Z} = [\boldsymbol{\mathcal{Z}}]^T_{(3)}$. The third-order tensor of the polarimetric FDA-MIMO radar can be shown in Fig. 2.

Based on the constructed tensor $\boldsymbol{\mathcal{Y}}$ in (20), the problem of interest is to jointly estimate the target parameters in polarimetric FDA-MIMO radar, including the angle θ_p, range r_p and two polarization parameters γ_p and η_p, for $p = 1 \cdots, P$.

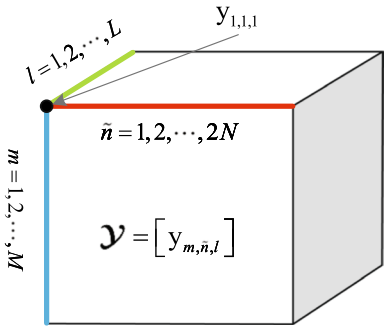

Fig. 2 The $M \times 2N \times L$ tensor for polarimetric FDA-MIMO radar

3.2 Tucker tensor decomposition for joint angle, range and polarization estimation

In this section, Tucker tensor decomposition methods are explored for angle-range-polarization estimation in FDA-MIMO radar. We present two methods: Tucker covariance reconstruction (TCR) algorithm and Tucker signal subspace (TSS) algorithm.

3.2.1 Tucker covariance reconstruction (TCR) algorithm

According to the definition of the product of two tensors, a fourth-order tensor $\boldsymbol{\mathcal{R}} \in \mathbb{C}^{M\times 2N\times M\times 2N}$ for the observation tensor $\boldsymbol{\mathcal{Y}}$ can be calculated by

$$\boldsymbol{\mathcal{R}} = \frac{1}{L}\boldsymbol{\mathcal{Y}} \bullet_3 \boldsymbol{\mathcal{Y}}^{*} \tag{21}$$

Then the HOSVD of the tensor $\boldsymbol{\mathcal{R}}$ is calculated as

$$\boldsymbol{\mathcal{R}} = \boldsymbol{\varsigma} \times_1 \mathbf{U}_1 \times_2 \mathbf{U}_2 \times_3 \mathbf{U}_3 \times_4 \mathbf{U}_4 \tag{22}$$

where $\boldsymbol{\varsigma} \in \mathbb{C}^{M\times 2N\times M\times 2N}$ is the core tensor, and $\mathbf{U}_i$ for $i = 1, 2, 3, 4$ denote the left singular vector matrices of the i-module expansion of $\boldsymbol{\mathcal{R}}$, expressed as

$$[\boldsymbol{\mathcal{R}}]_{(i)} = \mathbf{U}_i \boldsymbol{\Sigma}_i \mathbf{V}_i^{H} \ (i = 1, 2, 3, 4) \tag{23}$$

with $\mathbf{U}_1 = \mathbf{U}_3^{*}$ and $\mathbf{U}_2 = \mathbf{U}_4^{*}$.

To eliminate the noise, a truncated HOSVD [38] of the tensor $\boldsymbol{\mathcal{R}}$, which only contain the signal subspace component, can be obtained as

$$\boldsymbol{\mathcal{R}}_s = \boldsymbol{\varsigma}_s \times_1 \mathbf{U}_{1s} \times_2 \mathbf{U}_{2s} \times_3 \mathbf{U}_{1s}^{*} \times_4 \mathbf{U}_{2s}^{*} \tag{24}$$

where $\boldsymbol{\varsigma}_s \in \mathbb{C}^{P\times P\times P\times P}$ is the core tensor. $\mathbf{U}_{1s} \in \mathbb{C}^{M\times P}$ and $\mathbf{U}_{2s} \in \mathbb{C}^{2N\times P}$ contain the column vectors of $\mathbf{U}_1$ and $\mathbf{U}_2$ corresponding to the P dominant singular values, respectively.

First, a reconstructed covariance matrix $\mathbf{R}_s \in \mathbb{C}^{2MN\times 2MN}$ is formed based on the tensor $\boldsymbol{\mathcal{R}}_s \in \mathbb{C}^{M\times 2N\times M\times 2N}$ in (24) by Hermitian unfolding, which is given by

$$\mathbf{R}_s = ((\mathbf{U}_{1s}\mathbf{U}_{1s}^{H}) \otimes (\mathbf{U}_{2s}\mathbf{U}_{2s}^{H}))\mathbf{R}((\mathbf{U}_{1s}\mathbf{U}_{1s}^{H}) \otimes (\mathbf{U}_{2s}\mathbf{U}_{2s}^{H}))^{*} \tag{25}$$

where $\mathbf{R}$ is the covariance matrix of the observation matrix $\mathbf{Y}$, which can be estimated from finite snapshots in practice, given by $\hat{\mathbf{R}} = \frac{1}{L}\mathbf{Y}\mathbf{Y}^{H}$. Actually, $\mathbf{U}_{is}$ $(i = 1, 2)$ is the left singular vector matrix of $[\boldsymbol{\mathcal{R}}_s]_{(i)}$ corresponding to the first P largest singular values on the diagonal element of $[\boldsymbol{\mathcal{R}}_s]_{(i)}$. Both $\mathbf{U}_{1s}\mathbf{U}_{1s}^{H}$ and $\mathbf{U}_{2s}\mathbf{U}_{2s}^{H}$ are unitary matrices.

Then, the eigenvalue decomposition (EVD) of $\mathbf{R}_s$ is performed which can be written as $\mathbf{R}_s = \mathbf{E}_s\boldsymbol{\Lambda}_s\mathbf{E}_s^{H} + \mathbf{E}_n\boldsymbol{\Lambda}_n\mathbf{E}_n^{H}$, where $\boldsymbol{\Lambda}_s$ is a diagonal matrix whose elements on the diagonal line are the P dominant eigenvalues. $\mathbf{E}_s \in \mathbb{C}^{2MN\times P}$ denotes the signal subspace containing the eigenvectors corresponding to the P eigenvalues. Also, $\boldsymbol{\Lambda}_n$ is a diagonal matrix with the remaining $2MN - P$ eigenvalues on its diagonal line, and $\mathbf{E}_n \in \mathbb{C}^{2MN\times(2MN-P)}$ represents the noise subspace which contains the eigenvectors corresponding to the $2MN - P$ eigenvalues. Therefore, the rangle, angle and polarization parameters of each target can be estimated from $\mathbf{E}_s$. Obviously, $\mathbf{E}_s$ spans the same signal subspace with $\mathbf{A}(\theta, r, \gamma, \eta)$ in (19). As a result, there exists a unique nonsingular full-rank matrix $\mathbf{T}$ such that $\mathbf{E}_s = \mathbf{A}(\theta, r, \gamma, \eta)\mathbf{T}$.

Next, some sub-matrices can be obtained by proper processing of $\mathbf{E}_s$, which is based on the shift invariance of $\mathbf{A}(\theta, r, \gamma, \eta)$ maintained by $\mathbf{E}_s$. Firstly, $\mathbf{E}_s \in \mathbb{C}^{2MN\times P}$ is divided into M blocks, each of which is a matrix of $2N \times P$. Since there exists shift invariance for both transmit and receive arrays, different parameters can be estimated by choosing the following different sub-matrices:

For angle estimation, the shift-invariance property of the receive array is exploited. Define two selection matrices $\mathbf{J}_{r1} = [\mathbf{I}_{N-1}, \mathbf{O}_{(N-1)\times 1}]$ and $\mathbf{J}_{r2} = [\mathbf{O}_{(N-1)\times 1}, \mathbf{I}_{N-1}]$, then we have

$$(\mathbf{I}_M \otimes \mathbf{J}_{r2} \otimes \mathbf{I}_2)\mathbf{A} = (\mathbf{I}_M \otimes \mathbf{J}_{r1} \otimes \mathbf{I}_2)\mathbf{A}\boldsymbol{\Phi}_r \tag{26}$$

where $\boldsymbol{\Phi}_r = \mathrm{diag}(\phi_{\mathrm{r1}}, \phi_{\mathrm{r2}}, \cdots, \phi_{\mathrm{rP}})$ is the rotational matrix associated with the receive array, $\phi_{rp} = e^{j2\pi(d_r/\lambda_0)\sin\theta_p}$. Thus we can construct two sub-matrices $\mathbf{E}_{r1} \in \mathbb{C}^{2M(N-1)\times P}$ and $\mathbf{E}_{r2} \in \mathbb{C}^{2M(N-1)\times P}$ with the first and last $2(N-1)$ rows of each block of $\mathbf{E}_s$, respectively, i.e.,

$$\mathbf{E}_{r1} = (\mathbf{I}_M \otimes \mathbf{J}_{r1} \otimes \mathbf{I}_2)\mathbf{E}_s \tag{27a}$$

$$\mathbf{E}_{r2} = (\mathbf{I}_M \otimes \mathbf{J}_{r2} \otimes \mathbf{I}_2)\mathbf{E}_s \tag{27b}$$

then

$$\begin{aligned}\mathbf{E}_{r2} &= (\mathbf{I}_M \otimes \mathbf{J}_{r2} \otimes \mathbf{I}_2)\mathbf{A}\mathbf{T}\\ &= (\mathbf{I}_M \otimes \mathbf{J}_{r1} \otimes \mathbf{I}_2)\mathbf{A}\boldsymbol{\Phi}_r\mathbf{T}\\ &= (\mathbf{I}_M \otimes \mathbf{J}_{r1} \otimes \mathbf{I}_2)\mathbf{E}_s\mathbf{T}^{-1}\boldsymbol{\Phi}_r\mathbf{T}\\ &= \mathbf{E}_{r1}\boldsymbol{\Psi}_r\end{aligned} \tag{28}$$

where $\boldsymbol{\Psi}_r = \mathbf{T}^{-1}\boldsymbol{\Phi}_r\mathbf{T}$ denotes the EVD of $\boldsymbol{\Psi}_r$, with $\boldsymbol{\Phi}_r$ and $\mathbf{T}^{-1}$ representing the eigenvalue and eigenvector matrices of $\boldsymbol{\Psi}_r$, respectively. Thus the estimate of the angle θ_p can be obtained from $\boldsymbol{\Phi}_r$.

For range estimation, the shift-invariance property of the transmit array is used. Define two selection matrices $\mathbf{J}_{t1} = [\mathbf{I}_{M-1}, \mathbf{O}_{(M-1)\times 1}]$ and $\mathbf{J}_{t2} = [\mathbf{O}_{(M-1)\times 1}, \mathbf{I}_{M-1}]$, then

$$(\mathbf{J}_{t2} \otimes \mathbf{I}_N \otimes \mathbf{I}_2)\mathbf{A} = (\mathbf{J}_{t1} \otimes \mathbf{I}_N \otimes \mathbf{I}_2)\mathbf{A}\boldsymbol{\Phi}_t \tag{29}$$

where $\boldsymbol{\Phi}_t = \mathrm{diag}(\phi_{\mathrm{t1}}, \phi_{\mathrm{t2}}, \cdots, \phi_{\mathrm{tP}})$ is the rotational matrix with respect to the transmit array, where ϕ_{tp} satisfies

$$\phi_{tp} = e^{j2\pi((d_t/\lambda_0)\sin\theta_p - (\Delta f/c)2r_p)}, \tag{30}$$

which contains both the range r_p and angle θ_p. Therefore, we, respectively, generate two sub-matrices $\mathbf{E}_{t1} \in \mathbb{C}^{2(M-1)N\times P}$ and $\mathbf{E}_{t2} \in \mathbb{C}^{2(M-1)N\times P}$ using the first and last $M-1$ blocks of $\mathbf{E}_s$, i.e.,

$$\mathbf{E}_{t1} = (\mathbf{J}_{t1} \otimes \mathbf{I}_N \otimes \mathbf{I}_2)\mathbf{E}_s \tag{31a}$$

$$\mathbf{E}_{t2} = (\mathbf{J}_{t2} \otimes \mathbf{I}_N \otimes \mathbf{I}_2)\mathbf{E}_s \tag{31b}$$

Thus we have

$$\begin{aligned}\mathbf{E}_{t2} &= (\mathbf{J}_{t2} \otimes \mathbf{I}_N \otimes \mathbf{I}_2)\mathbf{A}\mathbf{T} \\ &= (\mathbf{J}_{t1} \otimes \mathbf{I}_N \otimes \mathbf{I}_2)\mathbf{A}\boldsymbol{\Phi}_t\mathbf{T} \\ &= (\mathbf{J}_{t1} \otimes \mathbf{I}_N \otimes \mathbf{I}_2)\mathbf{E}_s\mathbf{T}^{-1}\boldsymbol{\Phi}_t\mathbf{T} \\ &= \mathbf{E}_{t1}\boldsymbol{\Psi}_t\end{aligned} \tag{32}$$

where $\boldsymbol{\Psi}_t = \mathbf{T}^{-1}\boldsymbol{\Phi}_t\mathbf{T}$ stands for the EVD of $\boldsymbol{\Psi}_t$, and $\boldsymbol{\Phi}_t$, with $\mathbf{T}^{-1}$ being the eigenvalue and eigenvector matrices of $\boldsymbol{\Psi}_t$, respectively. Upon the angle θ_p has been obtained from $\boldsymbol{\Phi}_r$, we can further calculate the estimate of the range r_p from $\boldsymbol{\Phi}_t$.

For polarization parameter estimation, let us define two selection vectors $\mathbf{J}_{v1} = [0, 1]$ and $\mathbf{J}_{v2} = [1, 0]$, then we have

$$(\mathbf{I}_M \otimes \mathbf{I}_N \otimes \mathbf{J}_{v2})\mathbf{A} = (\mathbf{I}_M \otimes \mathbf{I}_N \otimes \mathbf{J}_{v1})\mathbf{A}\boldsymbol{\Phi}_v \tag{33}$$

where $\boldsymbol{\Phi}_v = \mathrm{diag}(\phi_{\mathrm{v1}}, \phi_{v2}, \cdots, \phi_{\mathrm{vP}})$, and ϕ_{vp} is the ratio of the two elements of the p-th polarization vector,

$$\phi_{vp} = \frac{-\cos\gamma_p}{\sin\gamma_p \cos\theta_p e^{j\eta_p}} \tag{34}$$

which contains the angle θ_p and two polarization parameters γ_p and η_p. Thus, we form two sub-matrices $\mathbf{E}_{v1} \in \mathbb{C}^{MN\times P}$ and $\mathbf{E}_{v2} \in \mathbb{C}^{MN\times P}$ from the even and odd rows of $\mathbf{E}_s$, respectively, i.e.,

$$\mathbf{E}_{v1} = (\mathbf{I}_M \otimes \mathbf{I}_N \otimes \mathbf{J}_{v1})\mathbf{E}_s \tag{35a}$$

$$\mathbf{E}_{v2} = (\mathbf{I}_M \otimes \mathbf{I}_N \otimes \mathbf{J}_{v2})\mathbf{E}_s \tag{35b}$$

Then

$$\begin{aligned}\mathbf{E}_{v2} &= (\mathbf{I}_M \otimes \mathbf{I}_N \otimes \mathbf{J}_{v2})\mathbf{A}\mathbf{T} \\ &= (\mathbf{I}_M \otimes \mathbf{I}_N \otimes \mathbf{J}_{v1})\mathbf{A}\boldsymbol{\Phi}_v\mathbf{T} \\ &= (\mathbf{I}_M \otimes \mathbf{I}_N \otimes \mathbf{J}_{v1})\mathbf{E}_s\mathbf{T}^{-1}\boldsymbol{\Phi}_v\mathbf{T} \\ &= \mathbf{E}_{v1}\boldsymbol{\Psi}_v\end{aligned} \tag{36}$$

where $\boldsymbol{\Psi}_v = \mathbf{T}^{-1}\boldsymbol{\Phi}_v\mathbf{T}$, with $\boldsymbol{\Phi}_v$ and $\mathbf{T}^{-1}$ being the eigenvalue and eigenvector matrices of $\boldsymbol{\Psi}_v$, respectively. Since the angle θ_p has been obtained from $\boldsymbol{\Phi}_r$, we can further achieve the estimates of the two polarization parameters γ_p and η_p from $\boldsymbol{\Phi}_v$.

In the above analysis, $\boldsymbol{\Psi}_r$, $\boldsymbol{\Psi}_t$ and $\boldsymbol{\Psi}_v$ can be calculated from (28), (32) and (36), respectively, by

$$\begin{cases}\boldsymbol{\Psi}_r = \mathbf{E}_{r1}^{\dagger}\mathbf{E}_{r2} \\ \boldsymbol{\Psi}_t = \mathbf{E}_{t1}^{\dagger}\mathbf{E}_{t2} \\ \boldsymbol{\Psi}_v = \mathbf{E}_{v1}^{\dagger}\mathbf{E}_{v2}\end{cases} \tag{37}$$

where † denotes the pseudo-inverse operation of a matrix.

Finally, the estimates of angle θ_p, range r_p, polarization parameters γ_p and η_p for $p = 1, \cdots, P$, are calculated by

$$\hat{\theta}_p = \arcsin\left(-\frac{\lambda_0}{2\pi d_r}\mathrm{ang}(\phi_{\mathrm{rp}})\right) \tag{38}$$

$$\hat{r}_p = \frac{(2\pi(d_t/\lambda_0)\sin\hat{\theta}_p - \mathrm{ang}(\phi_{\mathrm{tp}}))\mathrm{c}}{4\pi\Delta f} \tag{39}$$

$$\hat{\gamma}_p = \arctan\left|\frac{1}{\phi_{vp}\cos\hat{\theta}_p}\right| \tag{40}$$

$$\hat{\eta}_p = \mathrm{ang}\left(-\frac{1}{\phi_{\mathrm{vp}}\cos\theta_{\mathrm{p}}}\right) \tag{41}$$

Parameter pairing: In the case of multiple targets, we observe that the EVDs of $\mathbf{\Psi}_r$, $\mathbf{\Psi}_t$ and $\mathbf{\Psi}_v$ share the same eigenvector matrix $\mathbf{T}^{-1}$ but may have different sort in columns due to the existence of noise. To correctly estimate the multi-target parameters, the following pairing procedure is proposed: First, perform the EVD of $\mathbf{\Psi}_r$ to obtain its eigenvector matrix $\mathbf{Q}$ which corresponds to the eigenvalue matrix $\mathbf{\Phi}_r$. Then, construct a new signal subspace matrix $\tilde{\mathbf{E}}_s = \mathbf{E}_s\mathbf{Q}$. Next, obtain the sub-matrices $\tilde{\mathbf{E}}_{t1}$, $\tilde{\mathbf{E}}_{t2}$ and $\tilde{\mathbf{E}}_{v1}$, $\tilde{\mathbf{E}}_{v2}$ from $\tilde{\mathbf{E}}_s$, respectively, and similarly calculate $\tilde{\mathbf{\Psi}}_t$ and $\tilde{\mathbf{\Psi}}_v$ according to (37). The diagonal elements of $\tilde{\mathbf{\Psi}}_t$ and $\tilde{\mathbf{\Psi}}_v$ contain the paired range and polarization parameters, which correspond to the angle parameter of the p-th target.

The steps of the proposed TCR algorithm for range, angle and polarization estimation is given in Alg. 1.

Algorithm 1 Tucker Covariance Reconstruction (TCR) Algorithm

1: Calculate the sample covariance tensor $\boldsymbol{\mathcal{R}}$ using (21) based on $\boldsymbol{\mathcal{Y}}$.
2: Perform the truncated HOSVD of $\boldsymbol{\mathcal{R}}$ in (22) to obtain $\boldsymbol{\mathcal{R}}_s$.
3: Reconstruct a covariance matrix $\mathbf{R}_s$ by the Hermitian unfolding of $\boldsymbol{\mathcal{R}}_s$ using (25).
4: Perform the EVD of $\mathbf{R}_s$ to obtain $\mathbf{E}_s$.
5: Obtain $\mathbf{E}_{r1}$ and $\mathbf{E}_{r2}$ from $\mathbf{E}_s$ and calculate $\mathbf{\Psi}_r$ according to (37).
6: Perform the EVDs of $\mathbf{\Psi}_r$ to obtain the eigenvalue matrix $\mathbf{\Phi}_r$ and corresponding eigenvector matrix $\mathbf{Q}$.
7: Similarly obtain $\tilde{\mathbf{E}}_{t1}$, $\tilde{\mathbf{E}}_{t2}$ and $\tilde{\mathbf{E}}_{v1}$, $\tilde{\mathbf{E}}_{v2}$ from $\tilde{\mathbf{E}}_s$, and calculate $\tilde{\mathbf{\Psi}}_t$ and $\tilde{\mathbf{\Psi}}_v$ according to (37).
8: Calculate θ_p, r_p, γ_p and η_p from the diagonal elements of $\mathbf{\Phi}_r$, $\tilde{\mathbf{\Psi}}_t$ and $\tilde{\mathbf{\Psi}}_v$ using (38), (39), (40), (41), respectively.

3.2.2 Tucker signal subspace (TSS) algorithm

Compared with the reconstruction of covariance matrix $\mathbf{R}_s \in \mathbb{C}^{2MN\times 2MN}$, the direct utilization of the tensor $\boldsymbol{\mathcal{R}}_s \in \mathbb{C}^{M\times 2N\times M\times 2N}$ can make better use of the multidimensional structure of tensors. From the structure of the Tucker signal subspace tensor $\boldsymbol{\mathcal{R}}_s$, we can see that it contains the signal subspaces corresponding to the transmit and receive steering matrices, from which the multiple parameters can be obtained by using the properties of shift invariance in both transmit and receive arrays, respectively.

At first, like the TCR algorithm, we calculate the fourth-order tensor $\boldsymbol{\mathcal{R}} \in \mathbb{C}^{M\times 2N\times M\times 2N}$ for $\boldsymbol{\mathcal{Y}}$ as $\boldsymbol{\mathcal{R}} = \frac{1}{L}\boldsymbol{\mathcal{Y}}\bullet_3\boldsymbol{\mathcal{Y}}^{*}$. Recall that the truncated HOSVD of $\boldsymbol{\mathcal{R}}$ is performed as

$$\boldsymbol{\mathcal{R}}_s = \boldsymbol{\varsigma}_s \times_1 \mathbf{U}_{1s} \times_2 \mathbf{U}_{2s} \times_3 \mathbf{U}_{1s}^{*} \times_4 \mathbf{U}_{2s}^{*} \tag{42}$$

where $\mathbf{U}_{1s} \in \mathbb{C}^{M\times P}$ and $\mathbf{U}_{2s} \in \mathbb{C}^{2N\times P}$ consist of the P dominant eigenvectors of $\mathbf{U}_1$ and $\mathbf{U}_2$, respectively. Obviously, $\mathbf{U}_{1s}$ and $\mathbf{A}_t(\theta, r)$ span the same signal subspace, so there exists a unique nonsingular full-rank matrix $\mathbf{T}_1$ satisfying $\mathbf{U}_{1s} = \mathbf{A}_t(\theta, r)\mathbf{T}_1$. Similarly, $\mathbf{U}_{2s}$ and $\tilde{\mathbf{A}}_r(\theta, \gamma, \eta)$ span the same signal subspace, and there also exists a unique nonsingular full-rank matrix $\mathbf{T}_2$ satisfying $\mathbf{U}_{2s} = \tilde{\mathbf{A}}_r(\theta, \gamma, \eta)\mathbf{T}_2$, where $\tilde{\mathbf{A}}_r(\theta, \gamma, \eta) = \mathbf{A}_r(\theta) \diamond \mathbf{V}(\theta, \gamma, \eta)$. Then we can, respectively, use the shift invariance properties to both transmit and receive arrays to estimate the angle, range and polarization parameters.

For angle estimation, according to the shift-invariance property of the receiving array, we have

$$(\mathbf{J}_{r2} \otimes \mathbf{I}_2)\tilde{\mathbf{A}}_r = (\mathbf{J}_{r1} \otimes \mathbf{I}_2)\tilde{\mathbf{A}}_r\boldsymbol{\Phi}_r \tag{43}$$

where $\mathbf{J}_{r1} = [\mathbf{I}_{N-1}, \mathbf{O}_{(N-1)\times 1}]$ and $\mathbf{J}_{r2} = [\mathbf{O}_{(N-1)\times 1}, \mathbf{I}_{N-1}]$, and the rotational matrix is $\boldsymbol{\Phi}_r = \mathrm{diag}(\phi_{\mathrm{r1}}, \phi_{\mathrm{r2}}, \cdots, \phi_{\mathrm{rP}})$ with $\phi_{rp} = e^{j2\pi(d_r/\lambda_0)\sin\theta_p}$. Thus, the sub-matrices $\mathbf{U}_{r1} \in \mathbb{C}^{2(N-1)\times P}$ and $\mathbf{U}_{r2} \in \mathbb{C}^{2(N-1)\times P}$ are, respectively, constructed by selecting the first $2(N-1)$ and last $2(N-1)$ rows of $\mathbf{U}_{2s}$, i.e.,

$$\mathbf{U}_{r1} = (\mathbf{J}_{r1} \otimes \mathbf{I}_2)\mathbf{U}_{2s} \tag{44a}$$

$$\mathbf{U}_{r2} = (\mathbf{J}_{r2} \otimes \mathbf{I}_2)\mathbf{U}_{2s} \tag{44b}$$

then

$$\mathbf{U}_{r2} = (\mathbf{J}_{r2} \otimes \mathbf{I}_2)\tilde{\mathbf{A}}_r\mathbf{T}_2 = (\mathbf{J}_{r1} \otimes \mathbf{I}_2)\tilde{\mathbf{A}}_r\boldsymbol{\Phi}_r\mathbf{T}_2 = (\mathbf{J}_{r1} \otimes \mathbf{I}_2)\mathbf{U}_{2s}\mathbf{T}_2^{-1}\boldsymbol{\Phi}_r\mathbf{T}_2 = \mathbf{U}_{r1}\mathbf{D}_r \tag{45}$$

where $\mathbf{D}_r = \mathbf{T}_2^{-1}\boldsymbol{\Phi}_r\mathbf{T}_2$. We see that $\boldsymbol{\Phi}_r$ is the eigenvalue matrix of $\mathbf{D}_r$. From the diagonal elements of $\boldsymbol{\Phi}_r$, we can estimate the angle θ_p for the p-th target.

For range estimation, according to the shift-invariance property of the transmit array, we have

$$\mathbf{J}_{t2}\mathbf{A}_t = \mathbf{J}_{t1}\mathbf{A}_t\boldsymbol{\Phi}_t \tag{46}$$

where $\mathbf{J}_{t1} = [\mathbf{I}_{M-1}, \mathbf{O}_{(M-1)\times 1}]$ and $\mathbf{J}_{t2} = [\mathbf{O}_{(M-1)\times 1}, \mathbf{I}_{M-1}]$. The rotational matrix is $\boldsymbol{\Phi}_t = \mathrm{diag}(\phi_{t1}, \phi_{t2}, \cdots, \phi_{tp})$, where $\phi_{tp} = e^{j2\pi((d_t/\lambda_0)\sin\theta_p - (\Delta f/c)2r_p)}$. Therefore, two sub-matrix $\mathbf{U}_{t1} \in \mathbb{C}^{(M-1)\times P}$ and $\mathbf{U}_{t2} \in \mathbb{C}^{(M-1)\times P}$ are constructed by using the first $M-1$ and last $M-1$ rows of $\mathbf{U}_{1s}$, respectively, i.e.,

$$\mathbf{U}_{t1} = \mathbf{J}_{t1}\mathbf{U}_{1s} \tag{47a}$$

$$\mathbf{U}_{t2} = \mathbf{J}_{t2}\mathbf{U}_{1s} \tag{47b}$$

then

$$\mathbf{U}_{t2} = \mathbf{J}_{t2}\mathbf{A}_t\mathbf{T}_1 = \mathbf{J}_{t1}\mathbf{A}_t\mathbf{\Phi}_t\mathbf{T}_1 = \mathbf{J}_{t1}\mathbf{U}_{1s}\mathbf{T}_1^{-1}\mathbf{\Phi}_t\mathbf{T}_1 = \mathbf{U}_{t1}\mathbf{D}_t \tag{48}$$

where $\mathbf{D}_t = \mathbf{T}_1^{-1}\mathbf{\Phi}_t\mathbf{T}_1$. We observe that $\mathbf{\Phi}_t$ is the eigenvalue matrix of $\mathbf{D}_t$. Since $\mathbf{\Phi}_t$ contains both the angle and range parameters, the range r_p can be calculated when θ_p has been estimated.

For polarization parameter estimation, the shift-invariance property of the receive array is utilized again, then we have

$$(\mathbf{I}_N \otimes \mathbf{J}_{v2})\tilde{\mathbf{A}}_r = (\mathbf{I}_N \otimes \mathbf{J}_{v1})\tilde{\mathbf{A}}_v\mathbf{\Phi}_v \tag{49}$$

where $\mathbf{J}_{v1} = [0, 1]$ and $\mathbf{J}_{v2} = [1, 0]$, and $\mathbf{\Phi}_v = \mathrm{diag}(\phi_{\mathrm{v1}}, \phi_{\mathrm{v2}}, \cdots, \phi_{\mathrm{vP}})$, with $\phi_{vp} = \frac{-\cos\gamma_p}{\sin\gamma_p \cos\theta_p e^{j\eta_p}}$ being the ratio of the first and second elements of the polarization vector $\mathbf{v}(\theta_p, \gamma_p, \eta_p)$. We select the even rows from $\mathbf{U}_{2s}$ to form the sub-matrix $\mathbf{U}_{v1} \in \mathbb{C}^{N\times P}$, and odd rows to generate the sub-matrices $\mathbf{U}_{v2} \in \mathbb{C}^{N\times P}$, i.e.,

$$\mathbf{U}_{v1} = (\mathbf{I}_N \otimes \mathbf{J}_{v1})\mathbf{U}_{2s} \tag{50a}$$

$$\mathbf{U}_{v2} = (\mathbf{I}_N \otimes \mathbf{J}_{v2})\mathbf{U}_{2s} \tag{50b}$$

then

$$\mathbf{U}_{v2} = \mathbf{J}_{v2}\tilde{\mathbf{A}}_r\mathbf{T}_2 = \mathbf{J}_{v1}\tilde{\mathbf{A}}_r\mathbf{\Phi}_v\mathbf{T}_2 = \mathbf{J}_{v1}\mathbf{U}_{2s}\mathbf{T}_2^{-1}\mathbf{\Phi}_v\mathbf{T}_2 = \mathbf{U}_{v1}\mathbf{D}_v \tag{51}$$

where $\mathbf{D}_v = \mathbf{T}_2^{-1}\mathbf{\Phi}_v\mathbf{T}_2$, and $\mathbf{\Phi}_v$ is the eigenvalue matrix of $\mathbf{D}_v$. Thus, γ_p and η_p can be calculated if θ_p has been obtained.

Therefore, the estimates of θ_p, r_p, γ_p and η_p for $p = 1, \cdots, P$, are obtained from the eigenvalues of $\mathbf{D}_r$, $\mathbf{D}_t$ and $\mathbf{D}_v$, and finally calculated by the above-given (38)-(41).

Parameter pairing: It is necessary to match the parameters of angle, range and polarizations for multiple targets in the proposed TSS algorithm. We note that $\mathbf{D}_t$ and $\mathbf{D}_r$ own different eigenvector matrices $\mathbf{T}_1^{-1}$ and $\mathbf{T}_2^{-1}$, so we cannot match them according to eigenvectors. Therefore, the pairing procedure is based on sorting the diagonal elements of $\mathbf{\Phi}_r$, $\mathbf{\Phi}_t$ and $\mathbf{\Phi}_v$ according to the criterion of

$$f(\hat{\theta}_p) = \underset{\hat{r},\hat{\gamma},\hat{\eta},}{\arg\max} \left\| \left(\mathbf{a}_t(\hat{\theta}_p, \hat{r}) \otimes \mathbf{a}_r(\hat{\theta}_p) \otimes \mathbf{v}(\hat{\theta}_p, \hat{\gamma}, \hat{\eta}) \right)^H [\mathcal{Y}]_{(3)}^T \right\|_2^2 \tag{52}$$

for $p = 1, 2, \cdots, P$.

The steps of the proposed TSS algorithm for range, angle and polarization estimation is given in Alg. 2.

Algorithm 2 Tucker Signal Subspace (TSS) Algorithm

1: Calculate the sample covariance tensor $\boldsymbol{\mathcal{R}}$ using (21) based on $\boldsymbol{\mathcal{Y}}$.
2: Perform the truncated HOSVD of $\boldsymbol{\mathcal{R}}$ in (22) as $\boldsymbol{\mathcal{R}}_s$, and obtain its left singular vector matrices $\mathbf{U}_{1s}$ and $\mathbf{U}_{2s}$.
3: Construct $\mathbf{U}_{r1}$ and $\mathbf{U}_{r2}$ based on (44), $\mathbf{U}_{t1}$ and $\mathbf{U}_{t2}$ based on (47), and $\mathbf{U}_{v1}$ and $\mathbf{U}_{v2}$ based on (50).
4: Calculate $\mathbf{D}_r$, $\mathbf{D}_t$ and $\mathbf{D}_v$ according to $\mathbf{D}_r = \mathbf{U}_{r1}^{\dagger}\mathbf{U}_{r2}$, $\mathbf{D}_t = \mathbf{U}_{t1}^{\dagger}\mathbf{U}_{t2}$ and $\mathbf{D}_v = \mathbf{U}_{v1}^{\dagger}\mathbf{U}_{v2}$, respectively.
5: Perform the EVD of $\mathbf{D}_r$, $\mathbf{D}_t$ and $\mathbf{D}_v$ to obtain the eigenvalue matrices $\boldsymbol{\Phi}_r$, $\boldsymbol{\Phi}_t$ and $\boldsymbol{\Phi}_v$, respectively.
6: Match the diagonal elements of $\boldsymbol{\Phi}_r$, $\boldsymbol{\Phi}_t$ and $\boldsymbol{\Phi}_v$ according to the parameter pairing criterion in (52).
7: Determine θ_p, r_p, γ_p and η_p using (38), (39), (40), (41), respectively.

3.3 Performance analysis

In this section, we analyze the computational complexity of the proposed algorithms, and provide the CRB of joint range, angle and polarization estimation in polarimetric FDA-MIMO radar.

3.3.1 Computational complexity

According to some basic computational complexities of the SVD algorithm and the subspace methods in [35, 41], we analyze the complexities of the two proposed algorithms. The main computational burden of the proposed TCR algorithm comes from the calculation of the covariance tensor, HOSVD, covariance reconstruction, eigenvalue decomposition and multi-parameter estimation. Among them, $\mathcal{O}\{(2MN)^2L\}$ results from the fourth-order covariance tensor calculation. $\mathcal{O}\{4(2M)^2N^2P\}$ results from the truncated HOSVD in tensor decomposition method. $\mathcal{O}\{(2MN)^3\}$ results from the covariance reconstruction. $\mathcal{O}\{(2MN)^2P\}$ results from the eigenvalue decomposition of the signal covariance matrix. $\mathcal{O}\{2M(N-1)(2P)^2+(2P)^3+P^3\}$, $\mathcal{O}\{2(M-1)N(2P)^2+(2P)^3+P^3\}$ and $\mathcal{O}\{MN(2P)^2+(2P)^3+P^3\}$ result from the estimation of angle, range and polarizations using shift-invariance method, respectively. Thus, the complexity of the proposed Tucker covariance reconstruction algorithm is $\mathcal{O}\{8M^3N^3+20M^2N^2P+4M^2N^2L+4(5MN-2M-2N)P^2+27P^3\}$. Similarly, the main computational burden of the proposed TSS algorithm is the calculation of the covariance tensor, HOSVD, eigenvalue decomposition, multi-parameter estimation and parameter pairing, in which $\mathcal{O}\{(N-1)(2P)^2+(2P)^3+P^3\}$, $\mathcal{O}[2(M-1)(2P)^2+(2P)^3+P^3\}$ and $\mathcal{O}\{M(2P)^2+(2P)^3+P^3\}$, respectively, result from the angle, range and polarization estimation exploiting the shift-invariance method. $\mathcal{O}\{P^3\}$ results from the pairing between the parameters. Thus, the complexity of the proposed Tucker signal subspace algorithm is $\mathcal{O}\{16M^2N^2P+4M^2N^2L+4(3M+N-3)P^2+28P^3\}$.

3.3.2 Cramér–Rao bound

Under the hypothesis of target scattering signals stochastic and unknown to the receiver, the performance bound of multi-parameter estimation can be provided by

deriving the expression of stochastic CRB [49–51]. The CRB of joint range, angle and polarization estimation in polarimetric FDA-MIMO radar can be given by

$$\mathbf{CRB} = \frac{\sigma}{2L}\left\{\mathrm{Re}\left[\left(\mathbf{D}^H\boldsymbol{\Pi}_A^{\perp}\mathbf{D}\right)\odot\left[\mathbf{1}_{4\times4}\otimes\left(\mathbf{P}\mathbf{A}^H\mathbf{R}^{-1}\mathbf{A}\mathbf{P}\right)^T\right]\right]\right\}^{-1} \tag{53}$$

where $\odot$ denotes the Hadamard product, and $\mathbf{1}_{4\times4}$ is a 4×4 matrix with all the entities are ones. $\boldsymbol{\Pi}_{\mathbf{A}}^{\perp} = \mathbf{I}_{2MN} - \mathbf{A}(\mathbf{A}^H\mathbf{A})^{-1}\mathbf{A}^H$ and $\mathbf{R} = \mathbf{A}\mathbf{P}\mathbf{A}^H + \sigma\mathbf{I}_{2MN}$, where $\mathbf{P} = E\left[\mathbf{B}\mathbf{B}^H\right]$ is the covariance matrix of target signals, and

$$\mathbf{D} = \left[\frac{\partial\mathbf{A}}{\partial\boldsymbol{\theta}}, \frac{\partial\mathbf{A}}{\partial\boldsymbol{r}}, \frac{\partial\mathbf{A}}{\partial\boldsymbol{\gamma}}, \frac{\partial\mathbf{A}}{\partial\boldsymbol{\eta}}\right] \tag{54}$$

is the partial derivative matrix of $\mathbf{A}$ with respect to $\boldsymbol{\theta}, \boldsymbol{r}, \boldsymbol{\gamma}$ and $\boldsymbol{\eta}$, with $\boldsymbol{\theta} = [\theta_1, \theta_2, \cdots, \theta_P]^T$, $\boldsymbol{r} = [r_1, r_2, \cdots, r_P]^T$, $\boldsymbol{\gamma} = [\gamma_1, \gamma_2, \cdots, \gamma_P]^T$, $\boldsymbol{\eta} = [\eta_1, \eta_2, \cdots, \eta_P]^T$. $\frac{\partial\mathbf{A}}{\partial\boldsymbol{\theta}} = \left[\frac{\partial\mathbf{a}_1}{\partial\theta_1}, \cdots, \frac{\partial\mathbf{a}_P}{\partial\theta_P}\right]$, $\frac{\partial\mathbf{A}}{\partial\boldsymbol{r}} = \left[\frac{\partial\mathbf{a}_1}{\partial r_1}, \cdots, \frac{\partial\mathbf{a}_P}{\partial r_P}\right]$, $\frac{\partial\mathbf{A}}{\partial\boldsymbol{\gamma}} = \left[\frac{\partial\mathbf{a}_1}{\partial\gamma_1}, \cdots, \frac{\partial\mathbf{a}_P}{\partial\gamma_P}\right]$, $\frac{\partial\mathbf{A}}{\partial\boldsymbol{\eta}} = \left[\frac{\partial\mathbf{a}_1}{\partial\eta_1}, \cdots, \frac{\partial\mathbf{a}_P}{\partial\eta_P}\right]$, where

$$\begin{aligned}\frac{\partial\mathbf{a}_p}{\partial\theta_p} = \Bigg[&\frac{\partial\mathbf{a}_t(\theta_p, r_p)}{\partial\theta_p}\otimes\mathbf{a}_r(\theta_p)\otimes\mathbf{v}(\theta_p,\gamma_p,\eta_p)\\ &+\mathbf{a}_t(\theta_p, r_p)\otimes\frac{\partial\mathbf{a}_r(\theta_p)}{\partial\theta_p}\otimes\mathbf{v}(\theta_p,\gamma_p,\eta_p)\\ &+\mathbf{a}_t(\theta_p, r_p)\otimes\mathbf{a}_r(\theta_p)\otimes\frac{\partial\mathbf{v}(\theta_p,\gamma_p,\eta_p)}{\partial\theta_p}\Bigg]\end{aligned} \tag{55a}$$

$$\frac{\partial\mathbf{a}_p}{\partial r_p} = \left[\frac{\partial\mathbf{a}_t(\theta_p, r_p)}{\partial r_p}\otimes\mathbf{a}_r(\theta_p)\otimes\mathbf{v}(\theta_p,\gamma_p,\eta_p)\right] \tag{55b}$$

$$\frac{\partial\mathbf{a}_p}{\partial\gamma_p} = \left[\mathbf{a}_t(\theta_p, r_p)\otimes\mathbf{a}_r(\theta_p)\otimes\frac{\partial\mathbf{v}(\theta_p,\gamma_p,\eta_p)}{\partial\gamma_p}\right] \tag{55c}$$

$$\frac{\partial\mathbf{a}_p}{\partial\eta_p} = \left[\mathbf{a}_t(\theta_p, r_p)\otimes\mathbf{a}_r(\theta_p)\otimes\frac{\partial\mathbf{v}(\theta_p,\gamma_p,\eta_p)}{\partial\eta_p}\right] \tag{55d}$$

The diagonal elements of the CRB matrix give the CRBs of the estimates of angle $\boldsymbol{\theta}$, range $\boldsymbol{r}$ and polarization parameters $\boldsymbol{\gamma}$ and $\boldsymbol{\eta}$.

4 Results and discussion

In this section, we present the numerical experiment results to illustrate the performance of the proposed Tucker tensor decomposition-based algorithms for joint angle-range-polarization estimation. Consider a polarimetric FDA-MIMO radar system with inter-sensor spacing $d_t = d_r = \lambda_0/2$. The carrier frequency of the first sensor is $f_0 = 10GHz$, and the linear frequency increment is $\Delta f = 5kHz$. The polarization mode is assumed to be elliptical polarized, and the polarization state of each target echo is different.

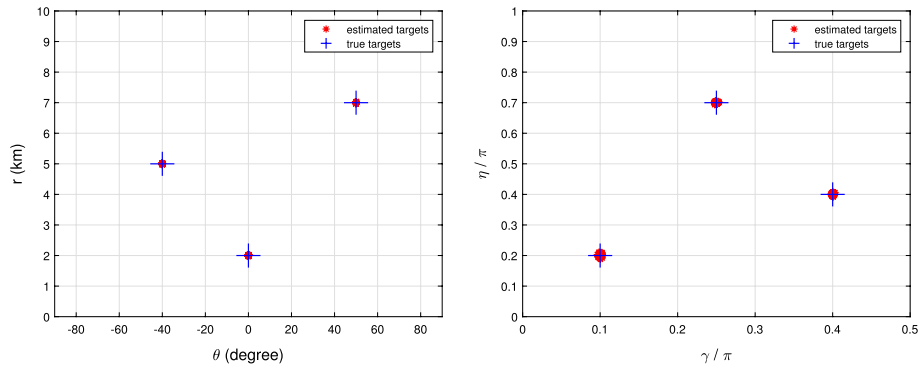

(a) angle and range (b) polarization parameters

Fig. 3 The range, angle and polarization estimation results using TCR algorithm. $M = 8$, $N = 8, P = 3, L = 100$, SNR $= 10$ dB, $(\theta, r) = (-40°, 5\,\text{km})(0°, 2\,\text{km})(50°, 7\,\text{km})$, $(\gamma, \eta) = (\pi/10, \pi/5)(2\pi/5, 2\pi/5)(\pi/4, 7\pi/10)$

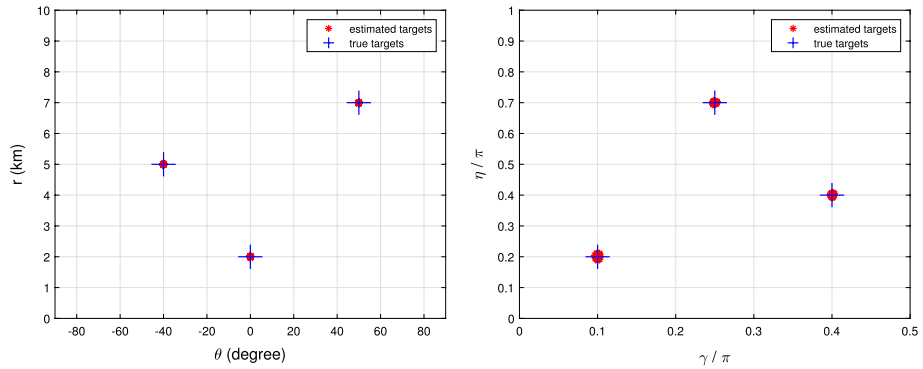

(a) angle and range (b) polarization parameters

Fig. 4 The range, angle and polarization estimation results using TSS algorithm. $M = 8$, $N = 8, P = 3, L = 100$, SNR $= 10$ dB, $(\theta, r) = (-40°, 5\,\text{km})(0°, 2, \text{km})(50°, 7\,\text{km})$, $(\gamma, \eta) = (\pi/10, \pi/5)(2\pi/5, 2\pi/5)(\pi/4, 7\pi/10)$

First, we verify the effectiveness of the proposed TCR and TSS algorithms. Assume that the polarimetric bistatic MIMO radar has $M = 8$ transmit sensors and $N = 8$ cross-dipole receive sensors. There are $P = 3$ uncorrelated targets which are distributed dispersedly, whose angle-range parameters are $(\theta, r) = (-40°,\ 5\,\text{km}), (0°,\ 2\,\text{km}), (50°,\ 7\,\text{km})$ and the polarization parameters are $(\gamma, \eta) = (\pi/10,\ \pi/5), (2\pi/5,\ 2\pi/5), (\pi/4,\ 7\pi/10)$. The signal-to-noise ratio (SNR) is 10dB and the number of snapshots is $L = 100$.

The simulation results of the TCR and TSS algorithms are shown in Figs. 3 and 4, respectively, with 100 Monte Carlo trials. From Figs. 3 and 4, it is observed that the estimates of angle, range and polarization parameters are close to their true values, and both the pairing methods given in Alg. 1 and Alg. 2 work well. The effectiveness and accuracies of the proposed algorithms can be verified from the simulation results.

Next, we compare the proposed TCR and TSS algorithms with the successive ESPRIT algorithm [35] and the successive propagator method [36] to evaluate the performance of range, angle and polarization estimation in FDA-MIMO radar. Here the root mean square error (RMSE) in estimating the parameter θ_p for the p-th target is calculated by

$$\mathrm{RMSE}_{\theta} = \frac{1}{P}\sum_{p=1}^{P}\sqrt{\frac{1}{t}\sum_{i=1}^{t}\left\{(\hat{\theta}_{i,p}-\theta_p)^2\right\}} \tag{56}$$

where t denotes the number of Monte Carlo experiments. The RMSEs of r_p, γ_p and η_p have the same calculation method as that of θ_p. The number of transmit sensors is $M = 6$, and the number of cross-dipole receive sensors is $N = 6$. The number of snapshots is $L = 5$. Assume that the SNR changes from -5 to 20dB, and three uncorrelated targets are distributed dispersedly with $(\theta, r) = (40°, 4\,\mathrm{km}), (-30°, 2\,\mathrm{km}), (10°, 5\,\mathrm{km})$ and $(\gamma, \eta) = (\pi/10, \pi/5)(\pi/5, 3\pi/5)(\pi/4, 2\pi/5)$. 500 Monte Carlo experiments are performed. The RMSEs of range, angle and two polarization parameters for different algorithms are shown in Fig. 5. It reveals that with the increase in SNR, the performance of the four algorithms is improved. The estimation accuracies of the two proposed tensor based algorithms are higher than that of the matrix-based successive ESPRIT algorithm and the successive propagator method, especially when the number of snapshots is small ($L = 5$). It implies that in the proposed tensor-based methods, the inherent multidimensional structure of the array data is well reserved. However, the multidimensional data structure in the successive ESPRIT algorithm and successive propagator method is rearranged into a matrix by stacking operation, thus the original structural characteristics is

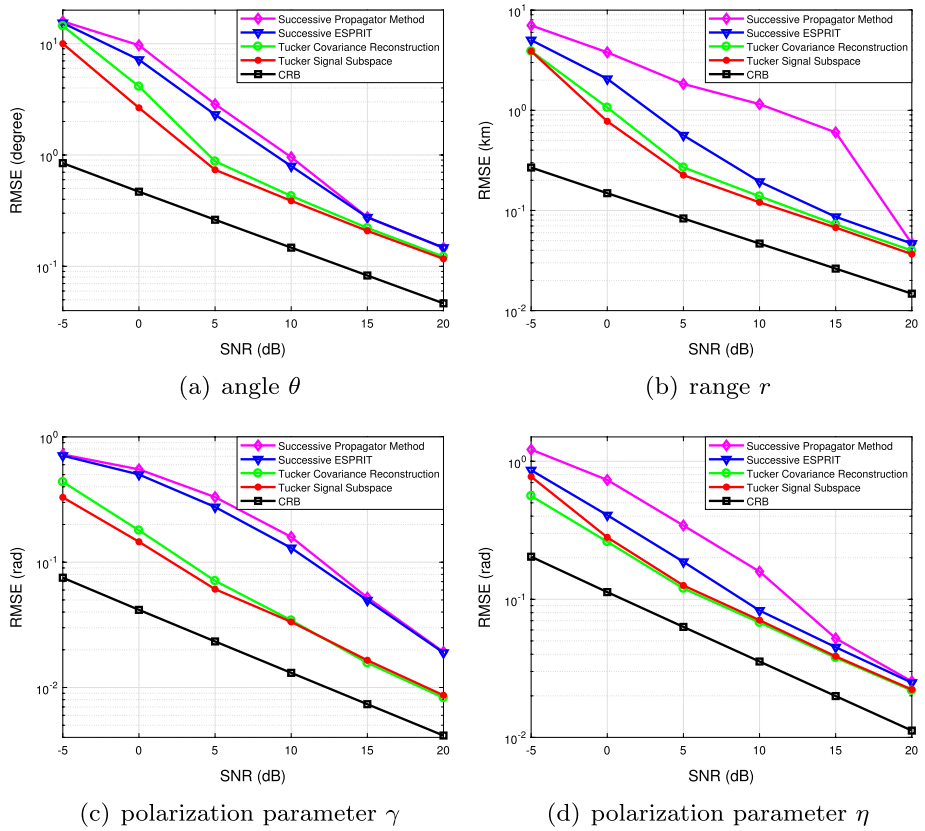

(a) angle θ (b) range r

(c) polarization parameter γ (d) polarization parameter η

Fig. 5 RMSE versus SNR for range, angle and polarization estimation using different methods. $M = 6$, $N = 6, P = 3, L = 5$ and 500 independent trials. $(\theta, r) = (40°, 4\,\mathrm{km}), (-30°, 2\,\mathrm{km}), (10°, 5\,\mathrm{km})$ and $(\gamma, \eta) = (\pi/10, \pi/5)(\pi/5, 3\pi/5)(\pi/4, 2\pi/5)$

destroyed, especially in a small number of snapshots. Therefore, the TSS and TCR algorithms achieve more accuracies than the successive ESPRIT algorithm and successive propagator method. Besides, the TSS algorithm is slightly superior to the TCR algorithm in accuracy by directly utilizing the signal subspace of Tucker tensor decomposition.

Then, we compare the performance of different algorithms in single snapshot environment. Assume that we conduct the simulation under the same conditions with the above experiment, except that the number of snapshots is $L = 1$. The RMSEs of the range, angle and polarization parameters with a single snapshot are shown in Fig. 6. We observe that the proposed TSS algorithm still works well even if the number of snapshots is one. In this case, the successive ESPRIT algorithm, the successive propagator method and the proposed TCR algorithm, which more or less depend on the calculation of covariance matrix, have lost the ability of parameter estimation when $L < P$. This shows the advantage of the proposed TSS algorithm by fully capturing the tensor nature for multiple parameter estimation in FDA-MIMO radar.

Next, we investigate the relationship between RMSE and the number of snapshots for different algorithms. The simulation conditions are identical with that of the above experiment except that SNR = 0 dB and the number of snapshots ranges from 1 to 29. The performance comparison of the angle, range and polarization parameters among the four algorithms is shown in Fig. 7. It is revealed that with the increase in the

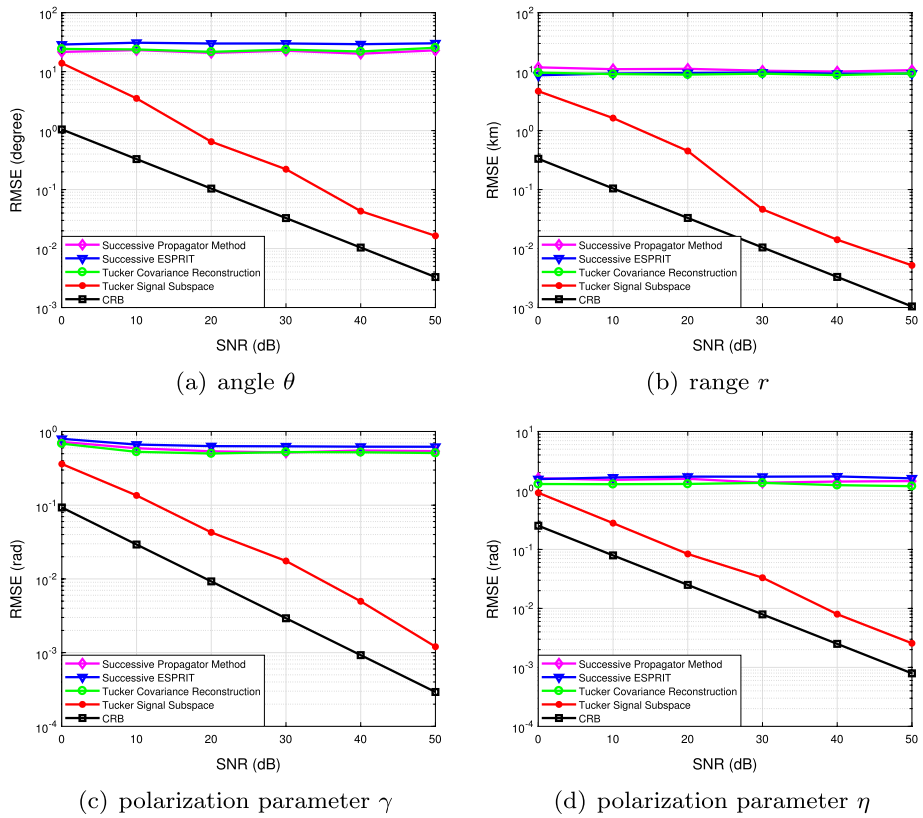

(a) angle θ (b) range r

(c) polarization parameter γ (d) polarization parameter η

Fig. 6 RMSE versus SNR for range, angle and polarization estimation with a single snapshot. $M = 6$, $N = 6, P = 3, L = 1$and 100 independent trials. $(\theta, r) = (40°, 4\,\text{km}), (-30°, 2\,\text{km}), (10°, 5\,\text{km})$ and $(\gamma, \eta) = (\pi/10, \pi/5)(\pi/5, 3\pi/5)(\pi/4, 2\pi/5)$

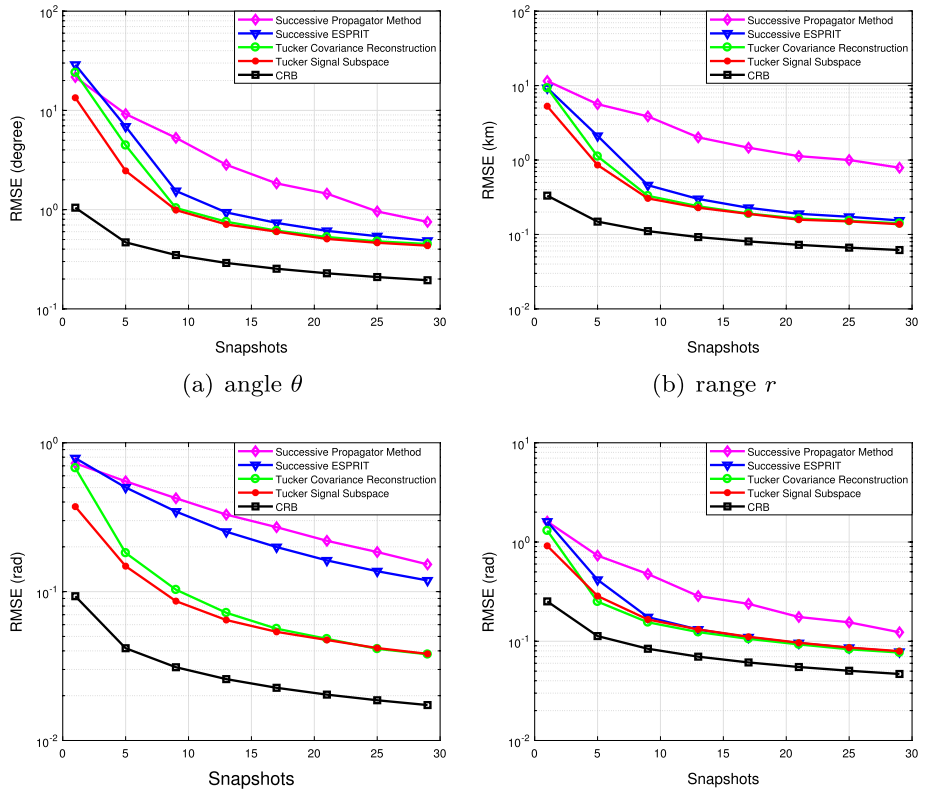

(a) angle θ (b) range r

(c) polarization parameter γ (d) polarization parameter η

Fig. 7 RMSE versus snapshot for range, angle and polarization estimation using different methods. $M = 6$, $N = 6, P = 3$, SNR =0 dB and 100 independent trials. $(\theta, r) = (40°, 4\,\text{km}), (-30°, 2\,\text{km}), (10°, 5\,\text{km})$ and $(\gamma, \eta) = (\pi/10, \pi/5)(\pi/5, 3\pi/5)(\pi/4, 2\pi/5)$

number of snapshots, the estimation accuracies of the four algorithms is improved. Also, when the number of snapshots is relatively small, the estimation accuracies of both the proposed TSS and TCR algorithms are higher than the successive ESPRIT algorithm and the successive propagator method. The TSS algorithm owns the highest accuracy among the four methods since it directly achieves the signal subspace from the fourth-order covariance tensor.

From the above several experiments we can observe that, by stacking the original multidimensional data into highly structured matrices may bring error accumulation and degrade the performance of multi-parameter estimation, especially when the number of snapshots is small. The proposed Tucker tensor decomposition based algorithms can utilize the inherent multidimensional structure characteristics in polarimetric FDA-MIMO radar, and have little damage to the original data structure. The TSS algorithm can better fit for the signal subspace estimation of multiple parameters in FDA-MIMO radar, so it can locate targets more accurately.

Moreover, we compare the running time of the TCR, TSS, successive ESPRIT and successive propagator method under two different array configurations: $M = 6, N = 6$, and $M = 30, N = 30$. Other simulation conditions are the same as those in the second experiment. From Table 1 we observe that when M and N are

Table 1 Running time comparison

Running time (s) / Array element / Method	$M = 6, N = 6$	$M = 30, N = 30$
TSS	0.2485915	3.459104
TCR	0.2673565	30.266638
successive ESPRIT	0.2419532	13.655026
successive propagator method	0.2280509	1.994791

relatively small, the TCR algorithm has slightly larger running time than the other three algorithms, the TSS and successive ESPRIT algorithms own similar and mediate

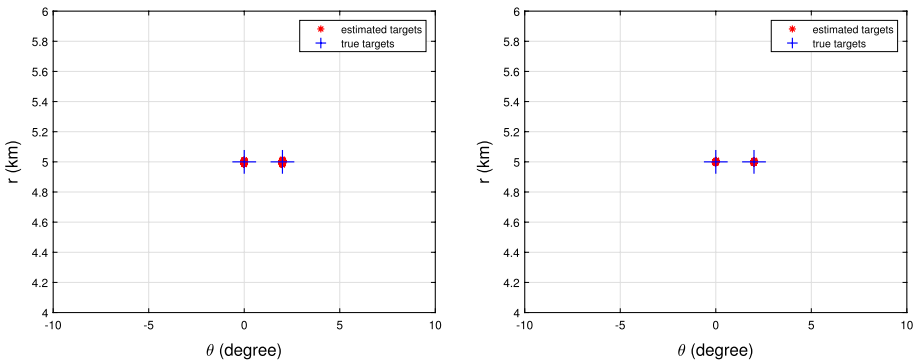

(a) TCR algorithm (b) TSS algorithm

Fig. 8 The range and angle estimation result when there are two closely spaced targets with same range and close angles. $M = 12, N = 12, P = 2$, SNR = 20 dB, $L = 100$ and 100 independent trials. $(\theta, r) = (0°, 5\,\text{km})(2°, 5\,\text{km}), (\gamma, \eta) = (\pi/10, \pi/5)(2\pi/5, 2\pi/5)$

running time, and the successive propagator method has the smallest running time. When M and N become large, the running time of the TCR algorithm significantly increases and is larger than the other three algorithms. The successive propagator method has the smallest running time but the lowest estimation accuracy. The TSS algorithm has a little larger running time than the successive propagator method but smaller running time than the TCR and successive ESPRIT algorithms. As a whole, the TSS algorithm can bring mediate complexity and higher estimation accuracy compared to the other methods.

Finally, we examine the estimates of range and angle when there are $P = 2$ closely spaced targets. Assume that $M = 12, N = 12$, SNR = 20dB and $L = 100$. The two targets are diversely polarized with polarization parameters $(\gamma, \eta) = (\pi/10, \pi/5)(2\pi/5, 2\pi/5)$. Also, the two targets have the same range and close angles $(\theta, r) = (0°, 5\,\text{km})(2°, 5\,\text{km})$. The estimation result of 100 Monte Carlo trials for range and angle estimation is shown in Fig. 8. It indicates that the proposed TSS and TCR algorithms can distinguish two targets having the same range and the close angles. Polarimetric FDA-MIMO radar can sense additional polarization information to improve target identification capability. By the use of polarization diversity in FDA-MIMO radar receiver, the angles and ranges of multiple closely spaced targets can be effectively identified with high-resolution.

Discussion: From the above experiment results, it is also note that there is still further improvement in accuracy to get closer to the CRB. For instance, based on the presented

Tucker tensor model of polarimetric FDA-MIMO radar, some effective noise suppression approach such as Tensor completion can be investigated, which we will conduct an in-depth research in future work.

5 Conclusion

In this article, we estimate range, angle and polarization parameters in polarimetric FDA-MIMO radar based on Tucker tensor decomposition. The three-order tensor signal model is constructed, and two tensor-based algorithms are, respectively, presented using the fourth-order covariance tensor decomposition. The complexity analysis and CRB for range, angle and polarizations are also provided. The proposed algorithms can effectively estimate the range-angle-polarization parameters with proper pairing. The tensor-based algorithms improve the performance compared with the matrix-based methods, especially under a small number of snapshots. This improvement results from the inherent multidimensional structure of FDA-MIMO radar data that is well reserved, which enables us to effectively reduce the accumulate error. In addition, by the use of the polarimetric FDA-MIMO radar that can sense additional polarization information, two targets with identical range and close angles can be effectively distinguished.

Abbreviations

FDA	Frequency diverse array
MIMO	Multiple-input multiple-output
TCR	Tucker covariance reconstruction
TSS	Tucker signal subspace
CRB	Cramér–Rao bound
ULA	Uniform linear array
MUSIC	Multiple signal classification
ESPRIT	Estimation of signal parameters via rotation invariance technique
HOSVD	Higher-order singular value decomposition (SVD)
TEM	Transverse electromagnetic mode
EVD	Eigenvalue decomposition
SNR	Signal-to-noise ratio
RMSE	Root mean square error

Acknowledgments
Not applicable.

Author contributions
ZQ, JH and L-YC proposed the tensor model and theoretical algorithms. ZQ carried out the simulation experiments. L-YC analyzed the estimation performance. JH improved the writing and edited the revised version. All authors read and approved the final manuscript.

Funding
This document is the results of the research funded by the National Natural Science Foundation of China under Grants 61371158 and 61771217, and the Natural Science Foundation of Jilin Province (CN) under Grant 20220101100JC and 20180101329JC.

Availability of data and materials
Data sharing not applicable to this article as no datasets were generated or analyzed during the current study.

Declarations

Ethics approval and consent to participate
Not applicable.

Consent for publication
Not applicable.

Competing interests
The authors declare that they have no competing interests.

Received: 30 October 2022 Accepted: 28 February 2023
Published online: 29 March 2023

References

1. E. Fishler, A. Haimovich, R. Blum, D. Chizhik, L. Cimini, R. Valenzuela, MIMO radar: an idea whose time has come. IEEE Radar conf. (Hawaii, USA, 2004), pp. 71–78
2. Y.D. Zhang, M.G. Amin, B. Himed, Joint DOD/DOA estimation in MIMO radar exploiting time-frequency signal representations. EURASIP J. Adv. Signal Process. **2012**, 102 (2012)
3. F. Zhang, C. Ji, Z. Zhang et al., Non-circular signal DOA estimation based on coprime array MIMO radar. EURASIP J. Adv. Signal Process. **2021**, 99 (2021)
4. P. Antonik, M.C. Wicks, H.D. Griffiths, C.J. Baker, Frequency diverse array radars. In 2006 IEEE Conference on Radar, 3 (2006)
5. W.-Q. Wang, Overview of frequency diverse array in radar and navigation applications. IET Radar, Sonar Navig. **10**(6), 1001–1012 (2016)
6. H. Chen, H. Shao, H. Chen, Angle-range-polarization-dependent beamforming for polarization sensitive frequency diverse array. EURASIP J. Adv. Signal Process. **2019**, 23 (2019)
7. Y. Dong, Frequency diverse array radar data processing. In: 2018 International Conference on Radar (RADAR), 1–5 (2018)
8. W.-Q. Wang, H.C. So, Transmit subaperturing for range and angle estimation in frequency diverse array radar. IEEE Trans. Signal Process. **62**(8), 2000–2011 (2014)
9. L. Huang, X. Li, P. C. Gong, et al. Frequency diverse array radar for target range-angle estimation. COMPEL Int. J. Comput. Math. Electr. Electron. Eng. (2016)
10. W.-Q. Wang, H. Shao, Range-angle localization of targets by a double-pulse frequency diverse array radar. IEEE J. Sel. Top. Signal Process. **8**(1), 106–114 (2014)
11. P.F. Sammartino, C.J. Baker, H.D. Griffiths, Frequency diverse MIMO techniques for radar. IEEE Trans. Aerosp. Electron. Syst. **49**(1), 201–222 (2013)
12. J. Xu, G. Liao, S. Zhu, L. Huang, H.C. So, Joint range and angle estimation using MIMO radar with frequency diverse array. IEEE Trans. Signal Process. **63**(13), 3396–3410 (2015)
13. J. Xu, G. Liao, Y. Zhang, H. Ji, L. Huang, An adaptive range-angle-Doppler processing approach for FDA-MIMO radar using three-dimensional localization. IEEE J. Sel. Top. Signal Process. **11**(2), 309–320 (2017)
14. B. Huang, A. Basit, R. Gui, W.-Q. Wang, Adaptive moving target detection without training data for FDA-MIMO radar. IEEE Trans. Veh. Technol. **71**(1), 220–232 (2022)
15. L. Lan, A. Marino, A. Aubry, A.D. Maio, G. Liao, J. Xu, Y. Zhang, GLRT-based adaptive target detection in FDA-MIMO radar. IEEE Trans. Aerosp. Electron. Syst. **57**(1), 597–613 (2021)
16. L. Lan, J. Xu, G. Liao, Y. Zhang, F. Fioranelli, H.C. So, Suppression of mainbeam deceptive jammer with FDA-MIMO radar. IEEE Trans. Veh. Technol. **69**(10), 11584–11598 (2020)
17. L. Lan, M. Rosamilia, A. Aubry, A.D. Maio, G. Liao, Single-snapshot angle and incremental range estimation for FDA-MIMO radar. IEEE Trans. Aerosp. Electron. Syst. **57**(6), 3705–3718 (2021)
18. R. Gui, B. Huang, W.-Q. Wang, Y. Sun, Generalized ambiguity function for FDA radar joint range, angle and Doppler resolution evaluation. IEEE Geosci. Remote Sens. Lett. **19**, 1–5 (2020)
19. J. Xiong, W.-Q. Wang, K. Gao, FDA-MIMO radar range-angle estimation: CRLB, MSE, and resolution analysis. IEEE Trans. Aerosp. Electron. Syst. **54**(1), 284–294 (2018)
20. Y. Yan, J. Cai, W.-Q. Wang, Two-stage ESPRIT for unambiguous angle and range estimation in FDA-MIMO radar. Digit. Signal Process. **92**, 151–165 (2019)
21. Y. Song, G. Zheng, G. Hu, A combined ESPRIT-MUSIC method for FDA-MIMO radar with extended range ambiguity using staggered frequency increment. Int. J. Antennas Propag. 2019, (2019)
22. Z. Xu, B. Huang, H. Hu, H. Chen and W. -Q. Wang, Ambiguity function-based ESPRIT algorithm for FDA-MIMO radar target localization. 2020 IEEE 11th Sensor Array and Multichannel Signal Processing Workshop (SAM). 1–4 (2020)
23. F. Liu, X. Wang, M. Huang et al., Joint angle and range estimation for bistatic FDA-MIMO radar via real-valued subspace decomposition. Signal Process. **185**(4), 108065 (2021)
24. J. Xu, W. -Q. Wang, C. Cui, R. Gui, Joint range, angle and Doppler estimation for FDA-MIMO radar. In: 2018 IEEE 10th Sensor Array and Multichannel Signal Processing Workshop (SAM). 499–503 (2018)
25. Z. Zhao, Z. Wang, Y. Sun, Joint angle, range and velocity estimation for bi-static FDA-MIMO radar. In: IEEE 2nd Advanced Information Technology, Electronic and Automation Control Conf. (IAEAC). 818–824 (2017)
26. W. Wu, F. Xi, Target localization for FDA-MIMO radar with random frequency increment via atomic norm minimization. In: 2019 IEEE MTT-S International Microwave Biomedical Conference (IMBioC). 1–4 (2019)
27. W. G. Tang, H. Jiang, Q. Zhang, Range-angle decoupling and estimation for FDA-MIMO radar via atomic norm minimization and accelerated proximal gradient. IEEE Signal Process. Lett. **27**, 366–370 (2020)
28. W. G. Tang, H. Jiang, S. Pang, Gridless angle and range estimation for FDA-MIMO radar based on decoupled atomic norm minimization. In: ICASSP 2019 - 2019 IEEE International Conference on Acoustics, Speech and Signal Processing (ICASSP). 4305–4309 (2019)
29. H. Jiang, D.F. Wang, C. Liu, Joint parameter estimation of DOD/DOA/polarization for bistatic MIMO radar. J. China Univ. Posts Telecommun. **17**(5), 32–37 (2010)
30. H. Jiang, D. F. Wang, C. Liu, Estimation of DOD and 2D-DOA and polarizations for bistatic MIMO radar. The 19th Annual Wireless and Optical Communications Conference (WOCC 2010). 1–5 (2010)
31. G. Zheng, M. Yang, B. Chen, W. Guo, Angle and polarization estimation using ESPRIT with polarimetric MIMO radar. In: IET International Conference on Radar Systems (Radar 2012). 1–4 (2012)

32. W. Guo, M. Yang, B. Chen, G. Zheng, Joint DOA and polarization estimation using MUSIC method in polarimetric MIMO radar. IET International Conference on Radar Systems (Radar 2012). 1–4 (2012)
33. H. Jiang, Y. Zhang, J. Li et al., A PARAFAC-based algorithm for multidimensional parameter estimation in polarimetric bistatic MIMO radar. EURASIP J. Adv. Signal Process. **2013**, 133 (2013)
34. H. Chen, H. Shao, W. Wang, Sparse reconstruction-based angle-range-polarization-dependent beamforming with polarization sensitive frequency diverse array. In 2016 IEEE International Conference on Acoustics, Speech and Signal Processing (ICASSP). 2891–2895 (2016)
35. B. Li, W. Bai, G. Zheng, Successive ESPRIT algorithm for joint DOA-range-polarization estimation with polarization sensitive FDA-MIMO radar. IEEE Access. **6**, 36376–36382 (2018)
36. J. Wang, S. Jiang, Angle-polarization-range estimation using sparse polarization sensitive FDA-MIMO radar with co-prime frequency offsets. IEEE Access. **7**, 146759–146771 (2019)
37. H. Chen, F. Ahmad, S. Vorobyov, F. Porikli, Tensor decompositions in wireless communications and MIMO radar. IEEE J. Sel. Top. Signal Process. **15**(3), 438–453 (2021)
38. M. Haardt, F. Roemer, G.D. Galdo, Higher-order SVD-based subspace estimation to improve the parameter estimation accuracy in multidimensional harmonic retrieval problems. IEEE Trans. Signal Process. **56**(7), 3198–3213 (2008)
39. L.R. Tucker, Some mathematical notes on three-mode factor analysis. Psychometrika. **31**(3), 279–311 (1966)
40. Y. Cheng, R. Yu, H. Gu et al., Multi-SVD based subspace estimation to improve angle estimation accuracy in bistatic MIMO radar. Signal Process. **93**(7), 2003–2009 (2013)
41. X. Wang, W. Wang, X. Li et al., A tensor-based subspace approach for bistatic MIMO radar in spatial colored noise. Sensors. **14**(3), 3897–3907 (2014)
42. F. Wen, X. Xiong, J. Su et al., Angle estimation for bistatic MIMO radar in the presence of spatial colored noise. Signal Process. **134**, 261–267 (2017)
43. F. Wen, Z. Zhang, G. Zhang, Y. Zhang, X. Wang, X. Zhang, A tensor-based covariance differencing method for direction estimation in bistatic MIMO radar with unknown spatial colored noise. IEEE Access. **5**, 18451–18458 (2017)
44. C. Mao, J. Shi, F. Wen, Target localization in bistatic EMVS-MIMO radar using tensor subspace method. IEEE Access. **7**, 163119–163127 (2019)
45. T.G. Kolda, B.W. Bader, Tensor decompositions and applications. SIAM Rev. **51**(3), 455–500 (2009)
46. L.D. Lathauwer, B.D. Moor, J. Vandewalle, A multilinear singular value decomposition. SIAM J. Matrix Anal. Appl. **21**(4), 1253–1278 (2000)
47. A. Nehorai, E. Paldi, Vector-sensor array processing for electromagnetic source localization. IEEE Trans. Signal Process. **42**(2), 376–398 (1994)
48. K.C. Tan, K.C. Ho, A. Nehorai, Linear independence of steering vectors of an electromagnetic vector sensor. IEEE Trans. Signal Process. **44**(12), 3099–3107 (1996)
49. P. Stoica, A. Nehorai, Performance study of conditional and unconditional direction-of-arrival estimation. IEEE Trans. Acoust. Speech Signal Process. **38**(10), 1783–1795 (1990)
50. M. Pesavento, A.B. Gershman, Maximum-likelihood direction-of-arrival estimation in the presence of unknown nonuniform noise. IEEE Trans. Signal Process. **49**(7), 1310–1324 (2001)
51. P. Stoica, E.G. Larsson, A.B. Gershman, The stochastic CRB for array processing: a textbook derivation. IEEE Signal Process. Lett. **8**(5), 148–150 (2001)

Publisher's Note